Paper ID: 130

A NEW METHOD FOR INDIVIDUAL IMPACT DAMAGE AND REPAIR ASSESSMENT ON COMPOSITE STRUCTURES BASED ON RESIDUAL STRENGTH ANALYSIS

Christoph P. Dienel[(1)], Tobias Wille[(1)], Julia Gerrero Santafe[(1)]

[(1)]German Aerospace Center, Lilienthalplatz 7, 38108 Braunschweig, Germany, Christoph.Dienel@dlr.de

KEYWORDS

Impact damage, CFRP, damage characterization, damage assessment, repair, residual strength

ABSTRACT

In this paper, a new method is introduced to support the maintenance process concerning decision making. Within this method, the individual damage and repair solutions can be assessed based on actual residual strength assessment by integrating three modules: the first is dedicated to the automatic identification of the impact damage through image segmentation of relevant damage features such as delaminations and fiber cracks captured with non-destructive methods; the second module enables an individual residual strength prediction of the damaged structure at hand, which is the basis for the decision whether immediate repair is required or not; finally, the third module provides a means of determining the load bearing capacity of a relevant bonded-repair concept with a given set of parameters. The results obtained by applying this new method including all three modules have been validated by experimental coupon tests.

1 INTRODUCTION

There are a variety of causes leading to impact damage during aircraft service life. Composite structures are especially sensitive to this damage type as their mechanical performance can be largely degraded. Low-velocity and low-energy impact events can originate the so-called barely visible impact damage. Although it can hardly be seen, sub-surface damage can establish, exerting a significant detrimental effect on the structure [1].

Various non-destructible inspection (NDI) methods have been developed to characterize such defects with sufficient detail. Ultrasonic inspection and x-ray based inspection methods have shown to be appropriate respectively for delamination and fiber crack detection, which are the most serious defects in composite structures [2].

Based on the inspection results and the requirements specified in the structure repair manual (SRM) provided by the original equipment manufacturer, the damage is assessed and the required steps to restore airworthiness are carried out [2].

Civil aviation authorities stipulate that airframe structures must follow a damage tolerant design, and that structural tests or validated analyses are required, to substantiate that the design objective has been met [3]. This, of course, applies to the design of intact and repaired structures, hence reflecting in the SRM requirements. Because of the many parameters that characterize a composite part (e.g. material, layup, laminate thickness, part geometry, etc.) and the various impact parameters (e.g. boundary conditions, impact energy, impactor shape, impact position, etc.) it becomes evident, that the number of tests tends to infinity. In order to reduce the test matrix, chosen parameter combinations are tested and curves are fitted through the data, in order to obtain a continuous relation between relevant parameters. To cope with the uncertainties associated with this method,

several reduction factors are applied to the fitted result, which gives rise to fairly or even unnecessarily conservative damage assessment and repair specifications.

In this paper a new method is suggested, where the damaged structure is assessed based on its actual characteristics (layup, part geometry, boundary conditions, damage distribution, etc.), and where a tailored bonded-repair concept is determined, to restore airworthiness. The method is comprised of three modules (see Figure 1) that will be presented here, which together pursue the objective of reducing excessive conservatism.

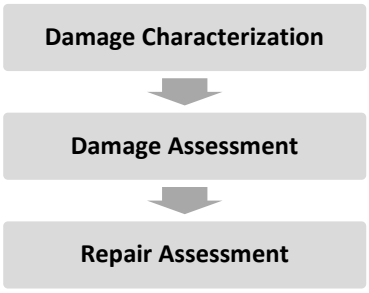

Figure 1: Method for individual impact damage and repair assessment

2 IMPACT DAMAGE CHARACTERIZATION

Depending on a variety of parameters (e.g. laminate thickness, boundary conditions, impact energy, impact velocity, etc.), different damage modes can install in composite structures due to impact events. Of the numerous damage modes arising, the most meaningful are fiber cracks, delaminations, and transversal matrix cracks, the latter however being only relevant as a starting point for delaminations [1,4,5].

Visual inspection is obviously insufficient to characterize impact damage, since fiber and matrix cracks, as well as delaminations per definition, are rather found inside the structure. In addition, impact damage modes can be very different regarding their geometry, position and consequently detectability. Thus, it is a common approach using complementary inspection methods to cope with this diversity. Destructive inspection methods have shown to be very instructive to study impact damage morphology and to be a means to validate non-destructive inspection result interpretation. On the other hand, NDI methods are indispensable for the evaluation of in-service airframe structures. References [6–9] present some of the key NDI methods for impact damage characterization in layered composite structures.

In the first module of the suggested method, two NDI techniques are adopted to acquire impact damage in composite specimens: ultrasonic and x-ray computer micro-tomography (micro-CT) inspection. Ultrasonic inspection is widely adopted to characterize delamination damage in layered composites [10–13]. Yet, this method is inadequate to detect matrix and fiber cracks. These, in turn, can be revealed by x-ray based methods, especially by the use of micro-CT [12,14,15]. It is worth noting that while micro-CT is appropriate for the investigation of rather small specimens, it is unsuitable for the inspection of large airframe components.

In the context of individual damage assessment, structure mechanics relevant damage features must be provided with sufficient accuracy. This objective is achieved in three data processing steps:

1. Data Segmentation: isolation of data representing damage from data describing the sound structure as well as other irrelevant features.

2. Data Classification: grouping and labeling of data

3. Data Interpretation: damage data complementation to yield a physically meaningful result, and reduction to reflect only relevant features for the subsequent damage assessment module.

Since the chosen NDI methods are dedicated to acquiring different damage modes, and because of the different data nature, the implementation of the processing steps mentioned above distinguishes.

2.1 Processing of Ultrasonic Inspection Results

Ultrasonic inspection consists of the through-the-thickness emission and reception of ultrasonic waves and their reflections. For each measurement point, the response is recorded in

terms of amplitude (i.e. the echo intensity) and time of flight (i.e. the time between emission and reception of an ultrasonic impulse). By knowing the speed of sound in the material under investigation, the depth of the echoing feature is derived from the time of flight. This results in two pictures: Amplitude-scan (C-scan) and Time-of-Flight-scan, or Depth-scan (D-scan), where each measuring point is represented by one pixel.

In the segmentation step, data processing is confined to a region of interest that generously spans the impact point vicinity. C-scan pixels below certain amplitude are regarded as noise and D-scan pixels representing depths coinciding with the specimen's front and back faces are excluded from further investigation. The remaining pixels describe relevant damage features inside the structure to be considered in the subsequent steps.

In the second step, these pixels are grouped according to their depth. Since delaminations are expected to establish at the interfaces between layers of different orientations [1], one would assume the pixel depth values to coincide with the known interfaces' depth. As suggested by Figure 2, the pixel value distribution is in fact rather discrete, concentrating at the true interface depth. However, pixel values present also some amount of scatter. This requires the definition of a band around the nominal interface depth, in order to include all pixels that presumably describe the same defect.

Finally, the segmentation and classification result is interpreted to achieve a physically significant and empirically consistent result. It is common knowledge, that the potential of the ultrasonic inspection method is limited by the shielding effect. It is understood as the signal attenuation originated by the first encountered defect which causes the echoes generated by underlying defects to be in the same order of magnitude as noise, thus not being interpretable. To obtain a more realistic defect shape, it is necessary to close the gap induced by the shielding effect. This is achieved by means of interpolation between the detected defect areas (Figure 3).

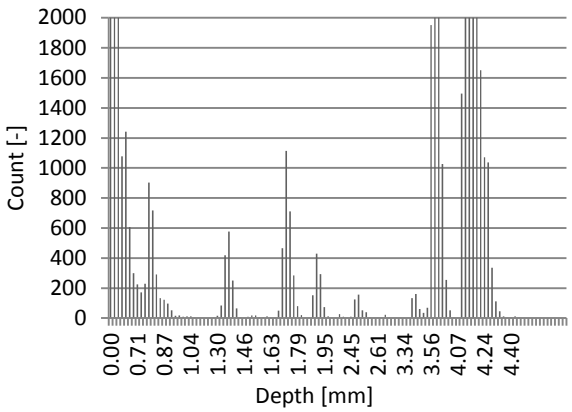

Figure 2: Ultrasonic histogram: depth vs. number of pixels.

2.2 Processing of Micro-CT Results

As a complementary means of characterizing relevant impact damage modes, micro-CT inspection is carried out. The micro-CT inspection result is a volume containing volumetric pixels (voxel) with different absorption amplitudes. Low amplitudes indicate voids (i.e. defects), whereas high amplitudes denote sound structure with higher x-ray absorption. These can be visualized as gray values or false color images.

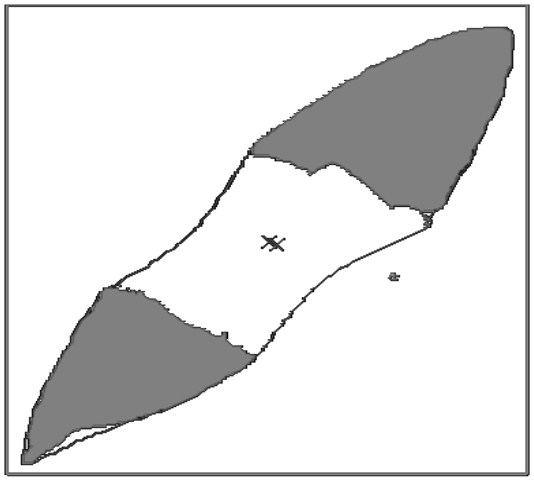

Figure 3: Detected delamination damage (filled purple areas) and interpolated "peanut-shaped" delamination geometry (purple contour) at the lowest interface of an impacted specimen.

Automatic micro-CT segmentation has proven to be a serious challenge with respect to impacted composites for a variety of reasons. For carbon

fiber reinforced plastics (CFRP) there is no detectable contrast between fibers and matrix. Besides that, impact induced deformation complicates defect segmentation, as damage features are not confined to a single voxel layer. In addition, the gray value distribution is very noisy and some defects can hardly be distinguished from noise artifacts, especially at the specimen's periphery Figure 4-A.

To cope with these difficulties, a linear shift invariant filter based on the Sobel-Feldman operator [16] is extended to the 3-dimensional space. A 3x3x3 kernel is applied to calculate gradient components in all three dimensions (G_x, G_y and G_z). Figure 4-B shows the through-the-thickness (i.e. z-direction) gradient component G_z.The gradient's weighted magnitude M (Figure 4-C) is defined by equation (1); a, b, and c are scalar factors.

$$M = \sqrt{a \cdot {G_x}^2 + b \cdot {G_y}^2 + c \cdot {G_z}^2} \qquad (1)$$

Different defects can be highlighted or suppressed, by changing the gradient components' contribution to the magnitude. For instance, setting $a = b = 0$ will highlight defects normal to the specimen's thickness, such as delaminations (Figure 4-D).

Complementary to this approach of localizing defect edges, an adaptive threshold-based filter is applied. The adaptive threshold is defined as the 2nd order polynomial, fitting the through-the-thickness gray values, reduced by a specific percentage. Voxel amplitudes below this adaptive threshold are temporarily labeled as "damage". The intersection of the defects detected by both approaches yields the segmentation result.

Defect classification into inter- or intralaminar damage is fulfilled by evaluating the orientation of the gradient vector $\underline{G} = (G_x, G_y, G_z)$. This can be described by two angles $\theta_1$and θ_2. θ_1 represents the angle of the gradient in z-direction against the gradient magnitude in the x,y-plane (equation (2)). Much stronger gradients in z-direction than those in the x,y-plane lead to $\theta_1$angles that tend towards 90°. A conditions is thus formulated, that classifies a defect as interlaminar damage if $\theta_1 > 75°$.

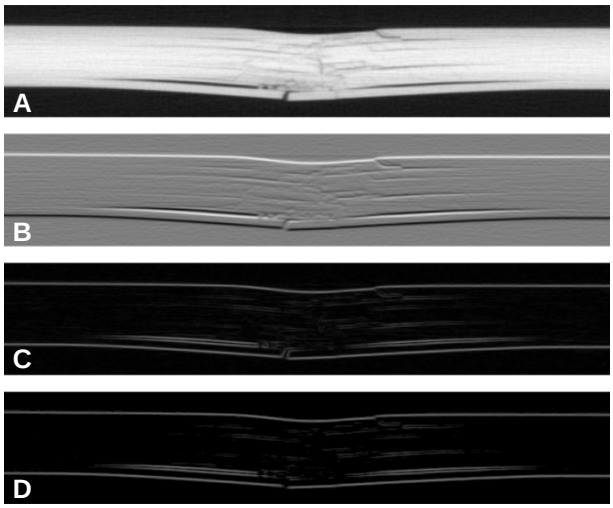

Figure 4: Micro-CT scan view of an impacted CFRP specimen at different processing states: A: unprocessed; B: gradient component in the z-direction; C: Magnitude for a=b=c=1; D: delamination edges and surfaces.

The angle θ_2 describes the gradient's orientation in the x,y-plane and is a measure by which fiber cracks can be distinguished from matrix cracks (equation (3)).

$$\theta_1 = \left| arctan\left(\frac{G_z}{\sqrt{{G_x}^2 + {G_y}^2}} \right) \right| \qquad (2)$$

$$\theta_2 = arctan\left(\frac{G_y}{G_x}\right) \qquad (3)$$

Although presenting a staggered geometry, fiber cracks can be interpreted as a straight line. In fact, from a structure mechanics point of view, only the straight connection of the crack tips matters, since this describes the area of reduced stiffness and the position where stress intensifications establish.

3 DAMAGE ASSESSMENT

The major step following damage characterization is dedicated to the residual strength prediction of the damaged structure (Figure 1), considering the actual impact damage. For this purpose, the structure is represented by a sufficiently discretized finite element model, encompassing all

relevant parameters, in order to mimic the main phenomena triggering the structural behavior.

The models are designed to predict both inter- and intralaminar damage propagation by applying cohesive zone modeling (CZM) and continuum damage mechanics (CDM), respectively. Parametric studies have been conducted to investigate the influence of CZM parameters on the result accuracy and on computation time [17], and the parameter set assigned to the models discussed here was chosen accordingly. The material parameters taken into account were determined through an extensive material characterization program. Orthotropic specimens composed by 13 ply-stacks and a 4.15mm thickness were impacted at 40J. The damage extent was characterized according to the methods described in the previous section and assigned to the finite element model. An explicit time integration method is adopted to calculate the models' behavior under quasi-static loading conditions.

To assess the capabilities of the damage assessment module, the simulation results are compared to those obtained from experiments on tension (TAI) and compression after impact (CAI) specimens.

3.1 Tension after Impact (TAI)

Impact damaged specimens loaded in tension experience severe strength loss when impact induced fiber cracks are found. This is attributed to the fact that the load is redirected, circumventing the intralaminar crack. Stress intensifications install at the crack tips which in turn can cause the initial crack to propagate. This is generally observed in 0° layers as these carry the highest loads. For single load path structures, such as the specimens considered here, fiber crack propagation generally represents catastrophic failure. Delaminations at a sufficient distance from the loading edges have only a minor effect on the residual tensile loading capability. This is because the transversal shear stresses are negligible when compared to the in-plane stresses. However, the combination of fiber cracks and delaminations can tremendously reduce the residual load-bearing capacity [18]. Owing to the shear-lag effect, sublaminates with fiber cracks can only take up loads at a certain distance from the adjacent delamination, which makes the detrimental influence of the impact site affect larger areas of the specimen than the extent of the fiber crack region itself.

The models integrated into the process chain (Figure 1) are defined to represent these relevant phenomena, enabling good failure load predictions. Figure 5 presents a comparison between experimentally determined residual strengths and those predicted by the proposed model, taking into account different damage mode combinations.

As depicted in Figure 5, the failure load of undamaged (virgin) specimens is slightly underestimated by less than 15%. This is attributed to the infinitely stiff boundary conditions acting upon the loading tabs as opposed to the actual experimental setup. Significant stress concentrations develop at the tabs, causing premature failure. For damaged structure models, this effect becomes negligible since loads tend to concentrate rather at the damage site. The results obtained by simulation suggest that the fracture load reduction is chiefly determined by the large fiber cracks (FC). The detrimental contribution of delaminations (D) and of the major matrix crack (MC) at the impact averted surface is found to be negligible. Considering all damage modes, an excellent failure load prediction is achieved (underestimation by less than 1%).

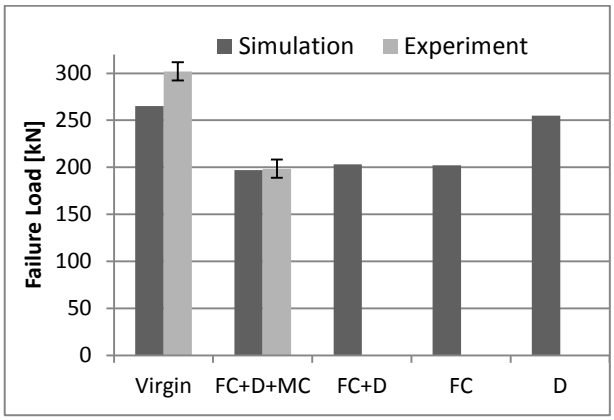

Figure 5: TAI failure loads for different damage states: experimental and simulation results.

Failure of tension loaded impact damaged specimens is characterized by fiber crack propagation perpendicularly to the loading direction in all 0° layers, accompanied by delamination growth that results from transverse shear and peel stresses at the spreading fiber crack front. This is exemplarily shown in Figure 6.

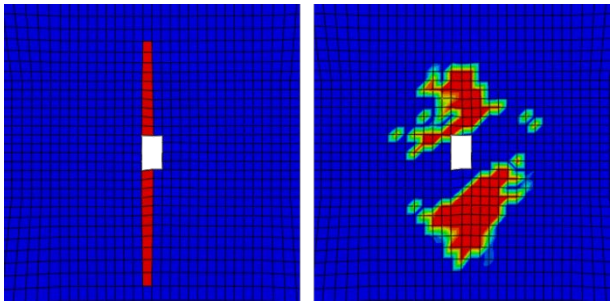

Figure 6: Fiber crack propagation (left) and delamination growth (right) in the fiber crack vicinity of a 0° layer.

3.2 Compression after Impact (CAI)

Compression after impact tests are performed according to the AITM1.0010 test standard [19]. This prescribes the specimen to be loaded in uniaxial compression, however inhibiting column buckling by the use of anti-buckling rails. Although column buckling is prevented, impact damaged specimens still experience stability failure. Delaminations resulting from an impact event divide the laminate into thin sublaminates. These – favored by the deformation due to impact – are prone to buckle under compressive loading. Because of different delamination shapes and varying sublaminate bending stiffness, the sublaminates experience different through-the-thickness displacements. This leads to peel stresses that promote delamination growth, and to bending loads that can cause fiber cracks to propagate.

The model proposed to replicate the CAI test is subjected to two analyses. The first is an Eigenvalue analysis where the buckling shapes of the sublaminates are determined. These are considered as initial geometric imperfections of the second analysis' model, where the failure load is finally calculated by taking into account local stability phenomena.

The results obtained from this approach are compared to experimental results in Figure 7.

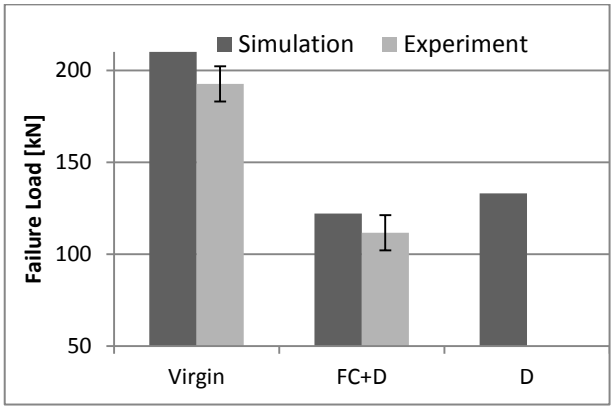

Figure 7: CAI failure loads for different damage states: experimental and simulation results.

Other than under tensile loading, simulation results attest significant loading capability reductions under compressive loads when regarding delamination damage. Considering the combination of fiber crack and delamination damage leads to further residual strength reduction. However, the fiber crack influence is less crucial. This is owed to the fact that out-of-plane stresses induced by buckling phenomena are fairly high, thus promoting delaminations to grow. On the other hand, fiber crack propagation is observed to set in at higher bending deflections, just prior to catastrophic failure. Although slightly overestimating the compressive failure load by less than 10%, the model provides a good estimate of the specimen's structural behavior.

4 DAMAGE REPAIR

The final step in the process chain presented in Figure 1 provides a means of predicting the residual load-bearing capacity of structures repaired according to an adjustable parameter set. For this purpose, a parametric model representing a scarfed bonded ply-by-ply repair is proposed. The geometrical parameters describing the repair region are the scarf angle, the inner radius and the overlapping length of the cover plies (Figure 8). For different parameter combinations, the model will return the respective failure load. This enables assessing the chosen repair parameter set in order to find a configuration that meets the effective design goal.

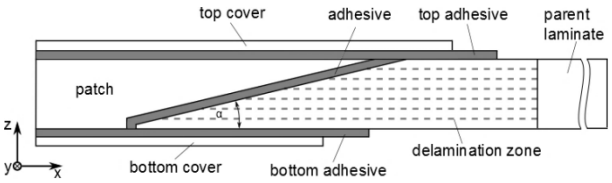

Figure 8: Schematic representation of the implemented scarfed bonded ply-by-ply repair.

For accurate prediction of the structural behavior, the finite element model is designed to represent the stress state and the respective phenomena occurring in the immediate vicinity of the bonded repair. Load transfer between adherents and the adhesive induces peel and transverse shear stresses which may lead to cohesive failure in both the adhesive and the laminate interfaces. To account for these phenomena, CZM is assigned to the adhesive and to the parent laminate's interfaces in the repair vicinity (Figure 8). Furthermore, intralaminar failure of fibers and matrix is regarded by applying the CDM.

Two sets of specimens were tested under tensile and compressive loading conditions presenting identical repair parameters. A scarf ratio of 1:30 was considered and cover plies were applied to the specimens' top and bottom sides as schematically shown in Figure 8.

Simulation results provide good approximations of the experimental results, however underpredicting the failure loads by less than 10% for the tension after repair (TAR) and less than 20% for the compression after repair (CAR) tests (Figure 9).

The crack running through the virgin tension specimen (TEN virgin) specimens has its origin in the stress concentration close to the loading tabs, and it propagates under 45° towards the opposite lateral edge. The damage establishing in repaired TAR specimens is slightly different. The fracture front connects the stress concentrations at the tabs with those establishing at the scarfed cutout under a 45° angle. The failure mode predicted by the repaired TAR model resembles that observed for virgin TEN specimen tests. This too is attributed to the boundary conditions that fail to represent the complex load introduction taking place in the experimental setup.

On the other hand, compression specimens present identical failure modes for both virgin (COM) and repaired (CAR) specimens. First, buckling sets in and due to high bending loads, the crack initiates at the clamping jaw. A similar behavior is also predicted by the COM and CAR models.

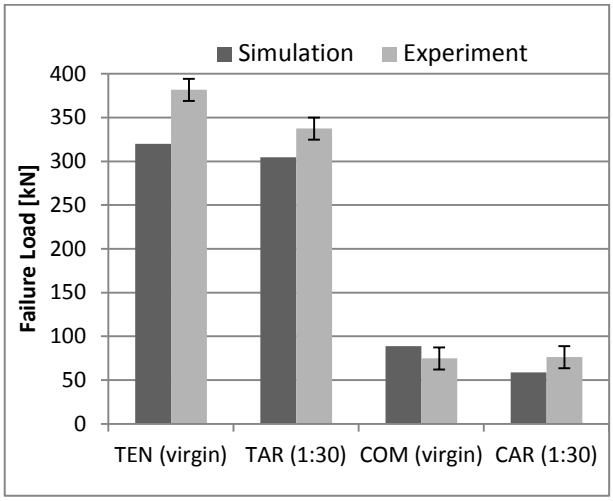

Figure 9: Tension and compression failure loads for virgin and repaired specimens: experimental and simulation results.

5 CONCLUSIONS

A method is suggested as a means of supporting decision making regarding handling impact damaged structures. This is composed of three modules dedicated to impact damage characterization, assessment, and repair.

The damage characterization module supports the segmentation, classification, and interpretation of NDI results, providing a physically meaningful description of the damage for further structure mechanical analysis.

The applied modeling strategy adopted in the second module enables accurate residual loading capacity prediction that is within the experimental scatter (less than 10%). This advocates that the model definition, as well as the impact damage characterization method, are appropriate for assessing the airworthiness of composite structures.

Likewise, the modeling strategy proposed in the third module yields a good approximation of the

experimental results obtained for repaired structures.

The proposed process chain points out that impact damage handling specifications can be given on the basis of automated assessment of individual damages. This clears the way for less conservative and yet safe structural designs, as current restrictive reduction factors can be relaxed. In addition, resource saving and an increase in aircraft availability can be achieved through demand-oriented repair.

ACKNOWLEDGEMENTS

The authors acknowledge the support provided by Mr. Wild (Quazar) and Prof. Grigat (TUHH Vision Systems) in the development of the damage characterization software *DaMapper*.

This study was conducted in the scope of the project "*Transferzentrum - MRO und Cabin Upgrade*" (grant number LAHH 144) which is funded by *Freie und Hansestadt Hamburg*.

REFERENCES

[1] Abrate S. *Impact on composite structures*. Cambridge University Press; 1998.

[2] Armstrong KB, Bevan LG, Cole WF II. *Care And Repair Of Advanced Composites*. 2nd ed. SAE International; 2005.

[3] Federal Aviation Administration. AC 25.571-1D - Damage Tolerance and Fatigue Evaluation of Structure – Document Information 2011.

[4] Cantwell WJ, Morton J. The impact resistance of composite materials — a review. *Composites* 1991;22:347–62. doi:10.1016/0010-4361(91)90549-V.

[5] Robin Olsson LEA. A review of some key developments in the analysis of the effects of impact upon composite structures. *Am. Soc. Test. Mater. Spec. Tech. Publ.*, vol. 1383, Seattle, WA: 1999, p. 12–28.

[6] Gao SL, Kim JK. Three-Dimensional Characterization of Impact Damage in CFRPs. *Key Eng Mater* 1998;141–143:35–54. doi:10.4028/www.scientific.net/KEM.141-143.35.

[7] Gros XE. Review of NDT Techniques for Detection of Low Energy Impacts in Carbon Reinforcements. *SAMPE J* 1995;31:29–34.

[8] Amaro AM, Reis PNB, de Moura MFSF, Santos JB. Damage detection on laminated composite materials using several NDT techniques. *Insight - Non-Destr Test Cond Monit* 2012;54:14–20. doi:10.1784/insi.2012.54.1.14.

[9] Garnier C, Pastor M-L, Eyma F, Lorrain B. The detection of aeronautical defects in situ on composite structures using Non Destructive Testing. *Compos Struct* 2011;93:1328–36. doi:10.1016/j.compstruct.2010.10.017.

[10] Aymerich F, Priolo P. Characterization of fracture modes in stitched and unstitched cross-ply laminates subjected to low-velocity impact and compression after impact loading. *Int J Impact Eng* 2008;35:591–608. doi:10.1016/j.ijimpeng.2007.02.009.

[11] Aymerich F, Meili S. Ultrasonic evaluation of matrix damage in impacted composite laminates. *Compos Part B Eng* 2000;31:1–6. doi:10.1016/S1359-8368(99)00067-0.

[12] Symons DD. Characterisation of indentation damage in 0/90 lay-up T300/914 CFRP. *Compos Sci Techno*l 2000;60:391–401. doi:10.1016/S0266-3538(99)00139-6.

[13] Hosur MV, Murthy CRL, Ramamurthy TS, Shet A. Estimation of impact-induced damage in CFRP laminates through ultrasonic imaging. *NDT E Int* 1998;31:359–74. doi:10.1016/S0963-8695(97)00053-4.

[14] Schilling PJ, Karedla BR, Tatiparthi AK, Verges MA, Herrington PD. X-ray computed microtomography of internal damage in fiber reinforced polymer matrix composites. *Compos Sci Technol* 2005;65:2071–8. doi:10.1016/j.compscitech.2005.05.014.

[15] Stoessel R, Wirjadi O, Godehardt M, Schlachter A-L, Liebscher A. Analysis of inner fracture surfaces in CFRP based on µ-CT image data, Wels, Austria: 2012.

[16] Duda RO, Hart PE. *Pattern Classification and Scene Analysis*. 1 edition. New York: Wiley; 1973.

[17] Dienel CP. Modeling the Behavior of Impact Induced Multiple Delaminations under Compressive Load. *Proc. Am. Soc. Compos. 2014-Twenty-Ninth Tech. Conf. Compos. Mater.*, San Diego, USA: DEStech Publications, Inc; 2014.

[18] Craven R, Sztefek P, Olsson R. Investigation of impact damage in multi-directional tape laminates and its effect on local tensile stiffness. *Compos Sci Technol* 2008;68:2518–25. doi:10.1016/j.compscitech.2008.05.008.

[19] Determination of Compression Strength After Impact. AIRBUS S.A.S.; 2005.